2017

A new energy storage system: Rechargeable potassium-selenium battery

Yajie Liu
University of Wollongong, yl327@uowmail.edu.au

Zhixin Tai
University of Wollongong, zt525@uowmail.edu.au

Qing Zhang
University of Wollongong, qz964@uowmail.edu.au

Hongqiang Wang
University of Wollongong, hw571@uowmail.edu.au

Wei Kong Pang
University of Wollongong, *Australian Nuclear Science and Technology Organisation*, wkpang@uow.edu.au

See next page for additional authors

Publication Details

Liu, Y., Tai, Z., Zhang, Q., Wang, H., Pang, W. Kong., Liu, H. Kun., Konstantinov, K. & Guo, Z. (2017). A new energy storage system: Rechargeable potassium-selenium battery. Nano Energy, 35 36-43.

A new energy storage system: Rechargeable potassium-selenium battery

Abstract
A new reversible and high-performance potassium-selenium (K-Se) battery, using confined selenium/carbonized-polyacrylonitrile (PAN) composite (c-PAN-Se) as cathode and metallic potassium as anode, is reported in this work. The PAN-derived carbon matrix could effectively confine the small Se molecules and provide a sufficient buffer for the volume changes. The reversible formation of small-molecule trigonal Se (Se1, P3121) phase could essentially inhibit the formation of polyselenides and account for outstanding electrochemical performance. The carbonate-based electrolyte further synergistically diminishes the shuttle effect by inhibiting the formation of polyselenides in the meantime. The as-prepared K-Se battery shows a reversible capacity of 1904 mAh cm¿3after 100 cycles at 0.2 C and rate retention of 89% from 0.1 to 2 C. In addition, the charge-discharge mechanism is also investigated via the combination of in-situ and ex-situ synchrotron X-ray diffraction (XRD), and Raman spectroscopy analysis. The results reveal that the introduction of K+ions leads to the cleavage of C-Se bonds, the rearrangement of selenium atoms, and the final formation of the main product K2Se. Moreover, the reversible formation of trigonal Se (Se1, P3121) phase was detected in the reaction with K+. These findings not only can advance our understanding of this family of batteries, but also provide insight into chemically-bonded selenium composite electrodes, which could give guidance for scientific research and the optimization of Se and S electrodes for the K-S, Na-S, Li-S, Na-Se, and Li-Se batteries.

Disciplines
Engineering | Physical Sciences and Mathematics

Publication Details
Liu, Y., Tai, Z., Zhang, Q., Wang, H., Pang, W. Kong., Liu, H. Kun., Konstantinov, K. & Guo, Z. (2017). A new energy storage system: Rechargeable potassium-selenium battery. Nano Energy, 35 36-43.

Authors
Yajie Liu, Zhixin Tai, Qing Zhang, Hongqiang Wang, Wei Kong Pang, Hua-Kun Liu, Konstantin K. Konstantinov, and Zaiping Guo

A New Energy Storage System: Rechargeable Potassium-Selenium Battery

Yajie Liu[a,1], Zhixin Tai[a,1], Qing Zhang[a,1], Hongqiang Wang[a], Wei Kong Pang[a,c], Hua Kun Liu[a], Konstantin Konstantinov[a] , Zaiping Guo[a,b]*

[a]Institute for Superconducting and Electronic Materials, Australian Institute for Innovative Materials, University of Wollongong, Innovation Campus, North Wollongong, New South Wales 2500, Australia.
*Corresponding author e-mail: zguo@uow.edu.au

[b]School of Mechanical, Materials and Mechatronics Engineering, University of Wollongong, North Wollongong, NSW 2500, Australia.

[c]Australian Centre for Neutron Scattering, Australian Nuclear Science and Technology Organisation, Locked Bag 2001, Kirrawee DC, NSW 2232, Australia.

1 These authors contributed equally to this work.

Abstract

A new reversible and high-performance potassium-selenium (K-Se) battery, using confined-selenium/carbonized-polyacrylonitrile (PAN) composite (c-PAN-Se) as cathode and metallic potassium as anode, is reported in this work. The PAN-derived carbon matrix could effectively confine the small Se molecules and provide a sufficient buffer for the volume changes. The reversible formation of small-molecule trigonal Se (Se_1, $P3_121$) phase could essentially inhibit the formation of polyselenides and account for outstanding electrochemical performance. The carbonate-based electrolyte further synergistically diminishes the shuttle effect by inhibiting the formation of polyselenides in the meantime. The as-prepared K-Se battery shows a reversible capacity of 1904 mAh cm^{-3} after 100 cycles at 0.2 C and rate retention of 89% from 0.1 C to 2 C. In addition, the charge-discharge mechanism is also

investigated via the combination of in-situ and ex-situ synchrotron X-ray diffraction (XRD), and Raman spectroscopy analysis. The results reveal that the introduction of K^+ ions leads to the cleavage of C-Se bonds, the rearrangement of selenium atoms, and the final formation of the main product K_2Se. Moreover, the reversible formation of trigonal Se (Se_1, $P3_121$) phase was detected in the reaction with K^+. These findings not only can advance our understanding of this family of batteries, but also provide insight into chemically-bonded selenium composite electrodes, which could give guidance for scientific research and the optimization of Se and S electrodes for the K-S, Na-S, Li-S, Na-Se, and Li-Se batteries.

Keywords: potassium-selenium batteries (K-Se batteries); small-molecule selenium; selenium cathodes; selenium/carbonized-PAN composite; potassium anode

Introduction

With the spotlight on renewable energy generation and electric vehicles, the demand for power supplies mainly based on batteries is rapidly increasing. Nevertheless, the energy density limitations and the high-cost of Li-ion batteries are compelling researchers to explore new battery systems. Alternative metal ion batteries based on earth-abundant metals, such as Na [1,2,3], K [4,5,6], Al [7], Mg [8,9,10], and Ca [11,12], have attracted increasing attention recently. Among them, although K is chemically overactive, several advantages of K anode cannot be ignored, such as its very low redox potential compared to the other metals ($E^\circ(K^+/K)$ = - 2.93 V, $E^\circ(Ca^{2+}/Ca)$ = -2.87 V, $E^\circ(Na^+/Na)$ = -2.71 V, $E^\circ(Mg^{2+}/Mg)$ = -2.27 V vs. standard hydrogen redox potential), abundant presence in nature, and low price. Moreover, recent studies have shown that K metal exhibits amazing properties in metal-oxygen batteries, having the lowest overpotential of all (less than 50 mV) [13,14]. Thus, focusing on the K-metal ion battery may lead to next-generation batteries with high capacity and low cost in the future.

The newly reported rechargeable potassium-sulfur battery could deliver a capacity of 329.3 mAh g^{-1} after 50 cycles [15], which is the highest capacity reported to date with potassium metal as anode. The cycling performance of the K-S battery, however, is inadequate, due to the production of polysulfides during cycling and the shuttle effect. Since Se and S exhibit similar atomic, molecular, and electrochemical properties, research on Se cathode in the Li-Se and Na-Se electrochemical systems has been conducted [16-22], not only to pursue a high-performance battery, but also to understand its theoretical and fundamental aspects. Compared to S (3470 mAh cm^{-3}), Se has a close theoretical volumetric capacity (3250 mAh cm^{-3}), but more stable electrochemistry compared to S [17]. The Se cathode features a theoretical gravimetric specific capacity of 675 mAh g^{-1}, 2-5 times higher than that of the traditional intercalation cathodes (*e.g.* Lithium Cobalt Oxide (LCO), Lithium Iron Phosphate (LFP), and Lithium Nickel Cobalt Aluminium Oxide (NCA)) which offsets its deficiency in terms of working voltage. As a result, a metal-Se battery is expected to deliver a comparable volumetric energy density to that of a metal-S battery and a higher gravimetric specific energy density than the metal-ion battery. In addition, the electronic conductivity of Se (1×10^{-3} $S \cdot m^{-1}$) is very much higher than that of S (5×10^{-28} $S \cdot m^{-1}$) [21]. Nevertheless, Se cathode still has many problems if we consider the K-Se system: (1) the reactivity of Se with an potassium metal is limited due to the large size of Se; (2) soluble intermediate polyselenides may shuttle to the anode, leading to rapid capacity fading during the discharge/charge cycling; (3) the relatively low voltage requires an alkali-metal as anode; and (4) the K-Se battery is a brand new battery system, so both an appropriate electrolyte and a suitable structure for the electrode to confine the Se particles need to be explored .

In this work, a novel potassium-selenium battery with a chemically-bonded carbonized-polyacrylonitrile (PAN)-Se (c-PAN-Se) composite as cathode material and K as anode is introduced. The c-PAN-Se was synthesized via the direct one-step sintering of a mixture of

PAN and Se in a sealed tube, instead of the traditional two-step selenium melt-diffusion into the porous carbon matrix. The initial bonds between C and Se in c-PAN-Se composite could facilitate Se uniform distribution, and strictly confine the Se in the PAN-derived carbon matrix on the atomic level. This provides a premise for the formation of smaller molecules of Se_1, which could essentially inhibit the formation of polyselenides Meanwhile, this easily-obtained porous carbonized-PAN matrix not only provide interconnected conductivity but also limit the volume changes to avoid the pulverization of particles. K-Se batteries with the cathode containing small molecules of Se_1 confined in the PAN-derived carbon could deliver high reversible capacity of 1904 mAh cm^{-3} or 396 mAh g^{-1} after 100 cycles, and good cycling performance (with 835 mAh cm^{-3} retained after 200 cycles at 5 C). The reaction mechanism and the state of the selenium electrode during cycling were investigated via ex-situ X-ray diffraction (XRD) and Raman spectroscopy, as well as by in-situ XRD analysis. It was found that the main discharge product, K_2Se, is formed after the initial bond cleavage between C and Se, and reversible small-molecule Se_1 was detected during cycling.

Experimental Section

Material Synthesis: The black and ultrafine chemically-bonded selenium/carbonized-PAN composite (c-PAN-Se) was prepared by heating a mixture of polyacrylonitrile (PAN, $(C_3NH_3)_n$, Aldrich) and selenium in a weight ratio of 1:1 at 600 ^oC for 8 h in a vacuum- sealed tube. A comparison sample, mixed c-PAN+Se, was synthesized by physically mixing the pyrolytic polyacrylonitrile with selenium. The pyrolytic polyacrylonitrile material (c-PAN) was obtained under the same conditions as for c-PAN-Se, but without the Se. The Se active matrial account for about 40% in composite, which is tested by TGA in Figure S1. The composite material (c-PAN-Se) and active material (Se) loading in this work are around 0.8-1.2 mg cm^{-2} and 0.3-0.5 mg cm^{-2}, respectively.

Materials characterization*:* The crystal structure of the powder products was examined by XRD (MMA GBC, Australia) with Cu Kα radiation. Fourier-transform infrared spectroscopy (FT-IR) and X-ray photoelectron spectroscopy (XPS) analysis were carried out to characterize the chemical bonds in samples. X-ray photoelectron spectroscopy (XPS) analysis was conducted on a VG Scientific ESCALAB 2201XL system with aluminium Kα X-ray radiation. A JEOL JSM-7500FA field-emission scanning electron microscope (FESEM) and a JEOL ARM-200F transmission electron microscope (TEM) were used to investigate the morphologies of the samples. Raman spectroscopy on an instrument (JOBIN YVON HR800) equipped with a 632.81 nm diode laser was used in the ex-situ analysis of the cells. A customized CR2032 coin cell for use in synchrotron X-ray powder diffraction (SXRPD) experiments was designed and made. In-situ synchrotron X-ray powder diffraction measurements were carried out at the Powder Diffraction beamline at the Australian Synchrotron, where the data were collected every 8 minutes during battery cycling at 0.5899 Å (as determined using LaB_6, NIST SRM 660b)

Electrochemical measurements: The c-PAN-Se composite electrode was assembled in an argon-filled glove box using coin-type (CR2032) cells. In order to prepare the cathode, a slurry containing 70wt% composite material, 20wt% Super P, and 10wt% poly(vinylidene difluoride) (PVDF) was dissolved in N-methyl-2-pyrrolidinone (NMP) solution. After that, the working electrodes were prepared by coating the slurry onto copper foil current collector, which was then dried at 60 ^{o}C for 24 h. A solution of 1 M potassium hexafluorophosphate (KPF_6) dissolved in ethylene carbonate (EC)/ propylene carbonate (PC) in a volume ratio of 1:1 was employed as the electrolyte. Cells with mixed c-PAN+Se and pure Se electrodes were also prepared using the same procedure. The coin cells were galvanostatically charged-discharged from 0.7 V to 2.3 V in potassium-selenium batteries using a Neware cell test instrument.

Results and discussion

The c-PAN-Se composite was simply fabricated via directly heating a mixture of selenium and PAN in a sealed tube. During the thermal treatment, the PAN was transformed into π-conjugated ring structures and formed covalent bonds with selenium species (Figure 1a). Specifically, the heat-treatment promoted the cyclization of PAN, resulting from bond-cleavage of nitrile groups and then bonding of the cleaved nitrogen to the carbon in the neighbouring groups [23]. This cyclization was accompanied by the dehydrogenation of PAN, resulting in a π-conjugated main chain, with the production of H_2Se as a by-product [24]. Subsequently, at relatively high temperature (600 ^{o}C), elemental selenium was turned into selenium free radicals, which then reacted with the PAN-derived carbon matrix and formed the final c-PAN-Se structure, in which the selenium, as shown in Figures 2b and 2c, forms covalent bonds with the carbon atoms or selenium local domains consisting of selenium chains of various lengths (Figure 1b). This possible reaction mechanism above was deduced based on the similar reaction process reported in sulfur-based composites [23,25,26]. This special covalently-bonded selenium (c-PAN-Se) results in Se that is uniformly distributed and confined in the c-PAN matrix, which plays a significant role in the formation of reversible small molecules of Se_1 to suppress the formation of polyselenides and stabilize the structure of the electrode materials to achieve long-term cyclability.

To confirm the reaction process and product formation of the chemically-bonded selenium composite, several characterizations have been conducted. Figure 2a shows the XRD patterns of elemental selenium, mixed c-PAN+Se, and c-PAN-Se. The pristine Se features a trigonal structure, and the mixed sample has the same diffraction peaks as selenium. Compared with the other samples, the c-PAN-Se has no sharp reflections, indicating an amorphous structure. Since the formation of C-Se bonds is the key evidence for judging whether Se has been incorporated into the PAN-based carbon matrix, Fourier-transform infrared (FT-IR)

spectroscopy was conducted to investigate the chemical bonds in c-PAN-Se. The most distinctive signals of selenium can be found in the low wavenumber region of 400-600 cm^{-1}, with weak peaks at 580, 520, and 436 cm^{-1} (Figure 2b inset).The strong band at 436 cm^{-1} could be assigned to the torsional vibrations of the hexagonal rings, coupled with the out-of-plane γ(C–Se) bending vibrations [27]. The peaks at 580 and 520 cm^{-1} correspond to C-Se bending vibrations [28,29]. Clearly, these peaks verify the existence of C-Se bonds in the c-PAN-Se. In addition, the FT-IR results also give information on the atomic configuration of the carbon matrix. The peaks of c-PAN at 1631 and 1269 cm^{-1} correspond to the symmetric stretching of C=C and C=N bonds, respectively, and the peak at 1396 cm^{-1} corresponds to the C-C bonds [23,30,31]. The shifting of the peaks in c-PAN-Se for the C=C and C=N bonds suggests the incorporation of Se into the c-PAN carbon matrix. Figure 2c presents the Se 3d XPS spectra for pristine Se and c-PAN-Se. For the pure Se, the Se $3d_{5/2}$ and $3d_{3/2}$ peaks are located at 56.1 and 55.2 eV, respectively, with a spin-orbit splitting of 0.86 eV, consistent with that of metallic selenium [19,32], while the Se $3d_{5/2}$ and $3d_{3/2}$ peaks shift to higher binding energy in c-PAN-Se. This shift is caused by changes in the electron cloud density of Se, indicating that the Se has formed bonds with carbon atoms in the composite to yield selenium-containing heterocyclic compounds. There are many reports in the literature of similar 3d peak shifts when Se is integrated with other atoms [17,19,33,34,35]. The C 1s spectrum (Figure 2d) can be divided into peaks for the following bonds: sp^2-type C=N bonds (286.8 eV) [30], C=C bonds (285.6 eV) [36], C–C bonds (285 eV) [37] and sp^2-type C–C bonds (284.3 eV) [30].

Transmission electron microscopy (TEM), field emission scanning electron microscopy (FESEM), and energy dispersive X-ray spectroscopy (EDX) were employed to investigate the morphology and element distribution of c-PAN-Se. The porous structure of c-PAN-Se with micro- and nanoscale pores and a relatively smooth surface is displayed in Figure S2a-b in the

Supporting Information. No isolated islands of Se can be observed on the carbonized-PAN surface. Scanning mode and Z-contrast transmission mode images of microsized c-PAN-Se are shown in Figure 3a-b. As in the high-resolution TEM image shown in Figure 3c, no fringes or any other well-ordered structure can be detected, suggesting the amorphous nature of the c-PAN-Se. This is consistent with the XRD results. Elemental mapping (Figure 3d-f) reveals the homogeneous distribution of selenium, carbon, and nitrogen in the composite.

The electrochemical performance of c-PAN-Se cathodes was examined in K-Se batteries. In the case of lithium-selenium and sodium-selenium batteries, it was reported that carbonate-based electrolyte could inhibit polyselenide formation with a single voltage plateau to avoid the shuttle effect compared with ether-based electrolyte [22]. In our work, we compared two different electrolytes (1 M KPF_6 in ethylene carbonate/ propylene carbonate (EC/PC) and 1 M KPF_6 in tetraethylene glycol dimethyl ether (TEGDME)) in order to choose the most appropriate one. It was found that the pristine selenium electrode shows a more serious shuttle effect in ether-based electrolyte than in carbonate-based electrolyte, which is concluded from the much more obvious orange-coloured polyselenides on glass-fibre separators and the drastic capacity drop in the cell with ether-based electrolyte (Figure S3a, b, d). Therefore, a carbonate-based electrolyte was employed for the c-PAN-Se cells. No colour can be found on the glass fibre separator for c-PAN-Se in EC/PC electrolyte, indicating that the shuttle effect could almost be ignored for c-PAN-Se electrode, even after long charge/discharge cycling. In our work, the voltage region between 0.7 and 2.3 V was selected for electrochemical testing in order to achieve better cycling performance (Figure S3e). Figure S4 shows the cyclic voltammograms (CVs) obtained at a scan rate of 0.1 mV s^{-1} between 0.7-2.3 V. A broad reduction peak due to the solid electrolyte interphase (SEI) formation is observed in the initial cathodic process with its peak value at 0.86 V, which disappears in the following cycles. From cycle 2, two reduction peaks appear in the cathodic process, corresponding to the

reactions from small molecular Se_1 to K_2Se that proceeds in two stages. There is an oxidation peak in the anodic process, corresponding to the reaction from K_2Se to Se_1. The voltages of the reduction peaks are consistent with those of the two voltage plateaus in the discharge curves (Figure 5c), indicating that there are two steps in the discharge process. The cycling stability of the c-PAN-Se composite was investigated at a current rate of 0.2 C (1 C = 3246 mAh cm^{-3} or 675 mAh g^{-1}) in a K-Se battery (Figure 4a). As for the selenium composite electrode, the capacity is calculated based on the weight of the selenium active material. The K-Se battery delivered a capacity of 3133 mAh cm^{-3} (652 mA h g^{-1}) in the first cycle, and then maintained a reversible capacity of 1904 mAh cm^{-3} (396 mAh g^{-1}) for 100 cycles. In contrast, the capacity of the pristine Se and physically mixed c-PAN+Se electrodes dropped to nearly zero after the first cycle (Figure 4b). The c-PAN-Se electrode initially shows a gradual increase in the specific capacity and then maintains a stable high capacity in the following cycles. The tendency towards increasing capacity could be considered as an activation process, in which more and more c-PAN-Se was activated and participated in the reaction. In addition to its excellent cycling stability, the c-PAN-Se composite also shows high rate capability in the potassium-selenium battery. As the current rate increases from 0.1 to 2 C, the c-PAN-Se electrode at 2 C maintains capacity retention of 89% relative to the second cycle capacity at 0.1 C in K-Se batteries. Even when charged/discharged at 10 C, it still delivers a reversible capacity of 673 mAh cm^{-3}. Figure 4d presents the charge/discharge curve of c-PAN-Se electrode. After increasing the current density by 10 times after 10 cycles, the cell still maintains the same capacity, only with a lower flat voltage plateau. The performance during prolonged cycling was investigated at the high current rate of 5 C with c-PAN-Se electrode. After 200 cycles, the capacity of 835 mAh cm^{-3} could be maintained, and a coulombic efficiency (CE) above 99% could be obtained after 15 cycles. The reversible nature of the potassium-selenium battery with high cycling and rate performance is demonstrated here. This high performance is associated with the well-confined small-molecule Se_1, which is

generated from the initial chemically-bonded atomic Se in PAN-derived carbon. The confined small molecules of Se_1 instead of Se_8 (Figure 5a) could essentially inhibit the formation of polyselenides and account for the outstanding cycling performance of c-PAN-Se. Similar conclusion was also reported on micropore-confined small-chain sulfur molecules and selenium confined in slit micropore carbon, which could inhibit the formation of polysulfides/polyselenides.[17] Specifically, the small Se_1 molecules can avoid the transition from Se_8 to Se_4^{2-} during the initial K uptake process, thereby preventing the formation of polyselenides (K_2Se_n, n = 4-8) upon discharging. Meanwhile, the space confinement of selenium in carbon pores leads to a favourable memory effect; viz., the in-situ formed K_2Se can only be transformed to small-molecule Se_1 rather than Se_8, which also inhibits the formation of polyselenides in the charging process. The electrochemical performance of c-PAN was investigated, as shown in Figure S5, in order to understand whether carbonized-PAN could contribute to the total capacity of the c-PAN-Se composite. In the same voltage range of 0.7-2.3 V, the specific capacity of c-PAN is around 15 mAh cm^{-3}, which can almost be ignored compared to the capacity of the c-PAN-Se.

To further analyse the electrochemical process or reaction mechanism in rechargeable K-Se batteries, ex-situ XRD with λ = 0.5899 Å was conducted to determine the reaction products between selenium and potassium (Figure 5a). After the third full discharge to 0.7 V vs. K/K^+, it can be seen that the main peaks at around 12.5°, 14.6°, and 21.6° are consistent with the standard pattern of K_2Se [CIF number: 60440], while the weak peaks located at 13.1°, 13.5°, and 18.7° correspond to K_2Se_2 [CIF number: 73172]. It could be concluded that the main product of the fully discharged selenium electrode is K_2Se. The selenium usually shows low reactivity with potassium metal in liquid electrolyte, which leads to an incomplete reaction between Se and K to produce K_2Se_2. This is analogous to the case of Na-S and K-S batteries, where Na_2S_x and K_2S_x ($x > 1$) are the discharge products [38, 15]. Interestingly, a small peak

associated with trigonal Se (Se_1, $P3_121$) was detected (Figure 5a) with a trigonal structure of 4 zig-zag pillars at the corners (Figure 5e), indicating the cleavage of the C-Se bonds and the formation of small selenium molecules. Ex-situ Raman spectra are presented to confirm this assumption, as shown in Figure 5b. After the first charge, a new small peak at around 237 cm^{-1} was detected, which is characteristic of trigonal selenium. Based on the above XRD and Raman spectroscopy, we can conclude that the C-Se bonds were broken, and then the selenium atoms reacted with K^+ (and electrons) to form K_2Se_2 or K_2Se during the discharge, with the K_2Se decomposing into Se_1 and K^+ (and electrons) during charge (Figure 5c). The overall reaction is a reversible reaction: $Se + 2K^+ \leftrightarrow K_2Se$. According to the electrochemical reaction above, the volume changes during charging/discharging can be calculated through the different densities of Se (4.81 g cm^{-3}) and K_2Se (2.29 g cm^{-3}). The volume expansion/shrinkage during charge and discharge is about 400%. This could be one of the reasons for the significant capacity drop of the pure selenium electrode, even in the carbonate-based electrolyte. Compared with bulk selenium, our uniform small-molecule confined composite exhibits excellent electrochemical performance, with the volume change from Se_1 to K_2Se being well controlled in the PAN-derived carbon matrix. This trigonal Se_1 ($P3_121$) is not only more active than the monoclinic Se_8 ($P12_1/n1$), which was reported for the Se cathode [20], but also able to decrease the strain due to the less absolute volume change during charging/discharging. In addition, with the protection of the carbonized PAN matrix, the excellent integrity and stability of the electrode could contribute to its outstanding long-term cycling performance. Figure 5d shows the contour plot corresponding to the in-situ synchrotron XRD spectra for the c-PAN-Se electrode, alongside the charge-discharge curves. Probably due to the incomplete reaction of Se with K, the low loading amount of active electrode material, and the limited diffractivity of the K_2Se/K_2Se_2 phases (as can be seen in Figure 5a), only the (101)/(011) reflection of trigonal Se ($P3_121$) phase is clearly observed,

showing good agreement with the ex-situ XRD results and suggesting the cleavage of C-Se bonds after the introduction of K^+.

Conclusions

In summary, high-performance potassium-selenium batteries with high reversibility are reported, with selenium confined in a porous carbonized-PAN matrix as cathode. The origin of the superior electrochemical behaviour is the confinement of small molecule Se_1 in the PAN-derived carbon matrix, which could inhibit the formation of polyselenides. Meanwhile, the conductive carbon matrix could also successfully deal with problems such as the large volume changes and low conductivity of selenium. The mechanism has been proposed based on the combination of in-situ and ex-situ XRD, the ex-situ Raman analysis, and electrochemical testing. We have detected the formation of small-molecule selenium (Se_1) and deduced that the cleavage of the C-Se bonds occurred in the initial cycles. This is the first fundamental research on the K-Se battery system, and, to the best of our knowledge, the K-Se battery shows the best cycling behaviour among all the K-ion batteries reported so far. Moreover, the outstanding cycling stability resulting from this composite, which features the confinement of small-molecule, may be applied to other similar battery systems, such as the potassium-sulfur battery. The relatively low voltage of the K-Se battery is the main drawback of this system, however reasonable energy density could be achieved by improving the capacity of the battery through optimization of the electrode composition and the electrolyte.

Acknowledgements

Support from the Australian Research Council (ARC) through Future Fellowship projects (FT150100109, FT160100251), and from Auto CRC 2020 (Project 1-117) are gratefully acknowledged. The authors would also like to thank the Electron Microscopy Centre (EMC)

at the University of Wollongong for the electron microscopy characterizations, and Dr. Tania Silver for critical reading of the manuscript and valuable remarks.

References

[1] A. Douglas, R. Carter, L. Oakes, K. Share, A.P. Cohn, C.L. Pint, ACS Nano 9 (2015) 11156-11165.

[2] A.P. Cohn, K. Share, R. Carter, L. Oakes, C.L. Pint, Nano Lett. 16 (2016) 543-548.

[3] L. Suo, Y.S. Hu, H. Li, M. Armand, L. Chen, Nat. Commun. 4 (2013) 1481.

[4] K. Share, A.P. Cohn, R. Carter, B. Rogers, C.L. Pint, ACS Nano 10 (2016) 9738-9744.

[5] Z. Jian, Z. Xing, C. Bommier, Z. Li, X. Ji, Adv. Energy Mater. 6 (2016) 1501874.

[6] I. Sultan, T. Ramireddy, M.M. Rahman, Y. Chen, A.M. Glushenkov, Chem. Commun. 52 (2016) 9279-9282

[7] M.C. Lin, M. Gong, B. Lu, Y. Wu, D.Y. Wang, M. Guan, M. Angell, C. Chen, J. Yang, B.J. Hwang, Nature 520 (2015) 324-328.

[8] H.S. Kim, T.S. Arthur, G.D. Allred, J. Zajicek, J.G. Newman, A.E. Rodnyansky, A.G. Oliver, W.C. Boggess, J. Muldoon, Nat. Commun. 2 (2011) 427.

[9] H.D. Yoo, I. Shterenberg, Y. Gofer, G. Gershinsky, N. Pour, D. Aurbach, Energy. Environ. Sci. 6 (2013) 2265-2279.

[10] S.Y. Ha, Y.W. Lee, S.W. Woo, B. Koo, J.S. Kim, J. Cho, K.T. Lee, N.S. Choi, ACS Appl. Mater. Interfaces 6 (2014) 4063-4073.

[11] A. Ponrouch, C. Frontera, F. Bardé, M.R. Palacín, Nature Materials 15 (2016) 169-172.

[12] K.A. See, J.A. Gerbec, Y.A. Jun, F. Wudl, G.D. Stucky, R. Seshadri, Adv. Energy Mater. 3 (2013) 1056-1061.

[13] X.D. Ren, Y.Y. Wu, J. Am. Chem. Soc. 135 (2013) 2923-2926.

[14] F.Y. Cheng, J. Chen, Chem. Soc. Rev. 41 (2012) 2172-2192.

[15] Q. Zhao, Y.X. Hu, K. Zhang, J. Chen, Inorg. Chem. 53 (2014) 9000-9005.

[16] J. Ding, H. Zhou, H.L. Zhang, T. Stephenson, Z. Li, D. Karpuzov, D. Mitlin, Energy Environ. Sci. (2017) DOI: 10.1039/c6ee02274j.

[17] (a) S. Xin, L. Yu, Y. You, H.P. Cong, Y.X. Yin, X.L. Du, Y.G. Guo, S.H. Yu, Y. Cui, J.B. Goodenough, Nano Lett. 16 (2016) 4560-4568; (b) S. Xin, L. Gu, N.H. Zhao, Y.X. Yin, L.J. Zhou, Y.G. Guo, L.J. Wan, J. Am. Chem. Soc. (134) 2012 18510-18513.

[18] Y. Cui, A. Abouimrane, J. Lu, T. Bolin, Y. Ren, W. Weng, C. Sun, V.A. Maroni, S.M. Heald, K. Amine, J. Am. Chem. Soc. 135 (2013) 8047-8056.

[19] C. Luo, Y. Xu, Y. Zhu, Y. Liu, S. Zheng, Y. Liu, A. Langrock, C. Wang, ACS Nano 7 (2013) 8003-8010.

[20] C.P. Yang, S. Xin, Y.X. Yin, H. Ye, J. Zhang, Y.G. Guo, Angew. Chem., Int. Ed. 52 (2013) 8363-8267.

[21] A. Abouimrane, D. Dambournet, K. W. Chapman, P. J. Chupas, W. Weng, K. Amine, *J. Am. Chem. Soc.* **2012**, *134*, 4505

[22] J. Guo, Z. Wen, Q. Wang, J. Jin, G. Ma, J. Mater. Chem. A 3 (2015) 19815-19821.

[23] T.H. Hwang, D.S. Jung, J.S. Kim, B.G. Kim, J.W. Choi, Nano Lett. 13 (2013) 4532-4538.

[24] H. Wang, S. Li, Z. Chen, H.K. Liu, Z. Guo, RSC Adv. 4 (2014) 61673-61678.

[25] J.L. Wang, J. Yang, J.Y. Xie, N.X. Xu, Adv. Mater. 14 (2002) 13-14.

[26] J. Wang, J. Yang, C. Wan, K. Du, J. Xie, N. Xu, Adv. Funct. Mater. 13 (2003) 6.

[27] K. Helios, A. Pietraszko, W. Zierkiewicz, H. Wojtowicz, D. Michalska, Polyhedron, 30 (2011) 2466-2472.

[28] J.A. Gómez Castaño, R.M. Romano, A.R. Salamanca, G. Amésquita, H. Beckers, H. Willner, C.O. Della Védova, J. Phys. Org. Chem. 29 (2016) 636-644.

[29] K. Grenader, M. Kind, L. Silies, A. Peters, J.W. Bats, M. Bolte, J. Mol. Struct. 1039 (2013) 61-70.

[30] X. Yu, J. Xie, J. Yang, H. Huang, K. Wang, Z. Wen, J. Electroanal. Chem. 573 (2004) 121-128.

[31] X.U. Yu, J.Y. Xie, Y. Li, H.J. Huang, C.Y. Lai, K. Wang, J. Power Sources 146 (2005) 335-339.

[32] J. Zhang, L. Fan, Y. Zhu, Y. Xu, J. Liang, D. Wei, Y. Qian, Nanoscale 6 (2014) 12952-12957.

[33] P.K. Babu, A. Lewera, J.H. Chung, R. Hunger, W. Jaegermann, N. Alonso-Vante, A. Wieckowski, E. Oldfield, J. Am. Chem. Soc. 129 (2007) 15140-15141.

[34] C. Luo, J. Wang, L. Suo, J. Mao, X. Fan, C. Wang, J. Mater. Chem. 3 (2015) 555-561.

[35] L. Zeng, X. Wei, J. Wang, Y. Jiang, W. Li, Y. Yu, J. Power Sources 281 (2015) 461-469.

[36] F. Bournel, C. Laffon, P. Parent, G. Tourillon, Surf. Sci. 350 (1996) 60-78.

[37] F.R. Diaz, C.O. Sanchez, M.A. del Valle, D. Radic, J.C. Bernede, Y. Tregouet, P. Molinie, Synth. Met. 110 (2000) 71-77.

[38] S. Xin, Y.X. Yin, Y.G. Guo, L.J. Wan, J. Adv. Mater. 26 (2014) 1261-1265.

Yajie Liu earned her B.S. degree in Chemical Engineering at the Beijing Institute of Technology, PR China in 2013. She is currently a Ph.D. candidate at the Institute for Superconducting and Electronic Materials (ISEM), University of Wollongong, Australia. Her research focus is on silicon anode for the lithium ion battery, and sulfur and selenium cathode for potassium ion batteries.

Zhixin Tai is currently a Ph.D. candidate at the Institute for Superconducting and Electronic Materials (ISEM), University of Wollongong, Australia. His research topics are focused on nano-structured materials for high-performance lithium ion and potassium ion batteries.

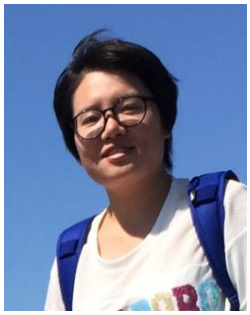

Qing Zhang is a Ph.D. candidate at the Institute for Superconducting and Electronic Materials (ISEM), University of Wollongong, Australia. His research topics are focused on smart design and synthesis of nanostructured anodes and cathodes for high-performance potassium ion batteries.

Hongqiang Wang received his Ph.D. degree from the Institute of Superconducting and Electronic Materials (ISEM), University of Wollongong, Australia. His research topics are focused on smart design and synthesis of nanostructured sulfur cathodes for high-performance

lithium sulfur batteries.

Wei Kong Pang received his Ph.D. in Applied Physics from Curtin University, Western Australia in 2011. After completion, he was first appointed as a postdoctoral research fellow in the Department of Chemistry at the National Taiwan University and the Department of Materials Engineering at Tatung University, Taiwan. In 2013 he joined the University of Wollongong and the Australian Nuclear Science and Technology Organisation as a postdoctoral research fellow. Recently he was awarded an Australian Research Council (ARC) Future Fellowship and is currently a senior research fellow at the Institute for Superconducting and Electronic Materials (ISEM), University of Wollongong.

Huakun Liu is a Distinguished Professor and a co-ordinator of the energy materials research program of the Institute for Superconducting and Electronic Materials (ISEM) at the Australian Institute of Innovative Materials, University of Wollongong. She was elected as a Fellow of the Australian Academy of Technological Science and Engineering in 2013. She has supervised 61 Ph.D. students to completion and 30 postdoctoral and visiting fellows. Her research has been focused on clean energy materials, materials science and engineering, and electrochemistry and applications

Konstantin Konstantinov is an Associate Professor in the Institute for Superconducting and Electronic Materials (ISEM), University of Wollongong. He has a career of more than 27 years as an internationally

recognized expert on the engineering of multifunctional ceramic nanocomposites for various applications and as a developer of mass-production nanotechnologies for ceramic synthesis. He is also working on several research directions including advanced energy storage composites.

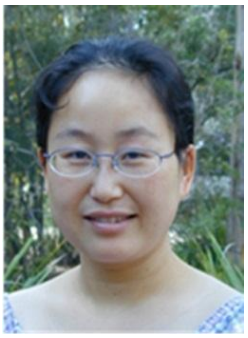

Zaiping Guo obtained her Ph.D. from the University of Wollongong in 2003. After her postdoctoral research with Prof. Huakun Liu at the Institute for Superconducting and Electronic Materials (ISEM), University of Wollongong, she joined the Faculty of Engineering in 2008. She is currently a senior professor and ARC Queen Elizabeth II (QEII) Fellow in the School of Mechanical, Materials & Mechatronic Engineering and the Institute for Superconducting & Electronic Materials, University of Wollongong. Her work is focused on practical applications of various nanomaterials as electrode materials for energy storage or conversion technologies, including rechargeable batteries, hydrogen storage, and supercapacitors.

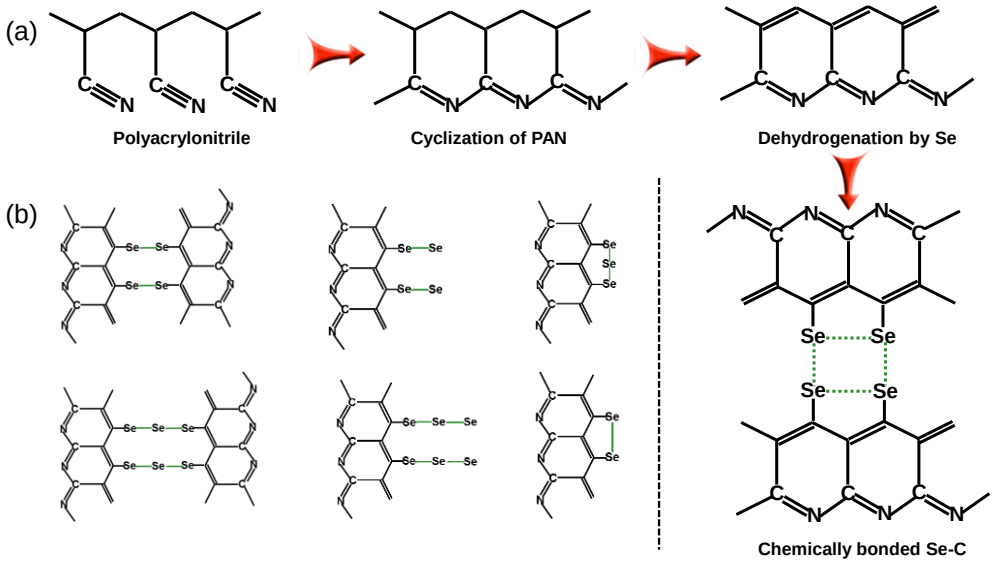

Figure 1. (a) Reaction mechanism and changes in the molecular structure during the carbonization of PAN and selenization between Se and c-PAN; (b) Possible molecular structures of the as-prepared chemically-bonded selenium/carbon composite.

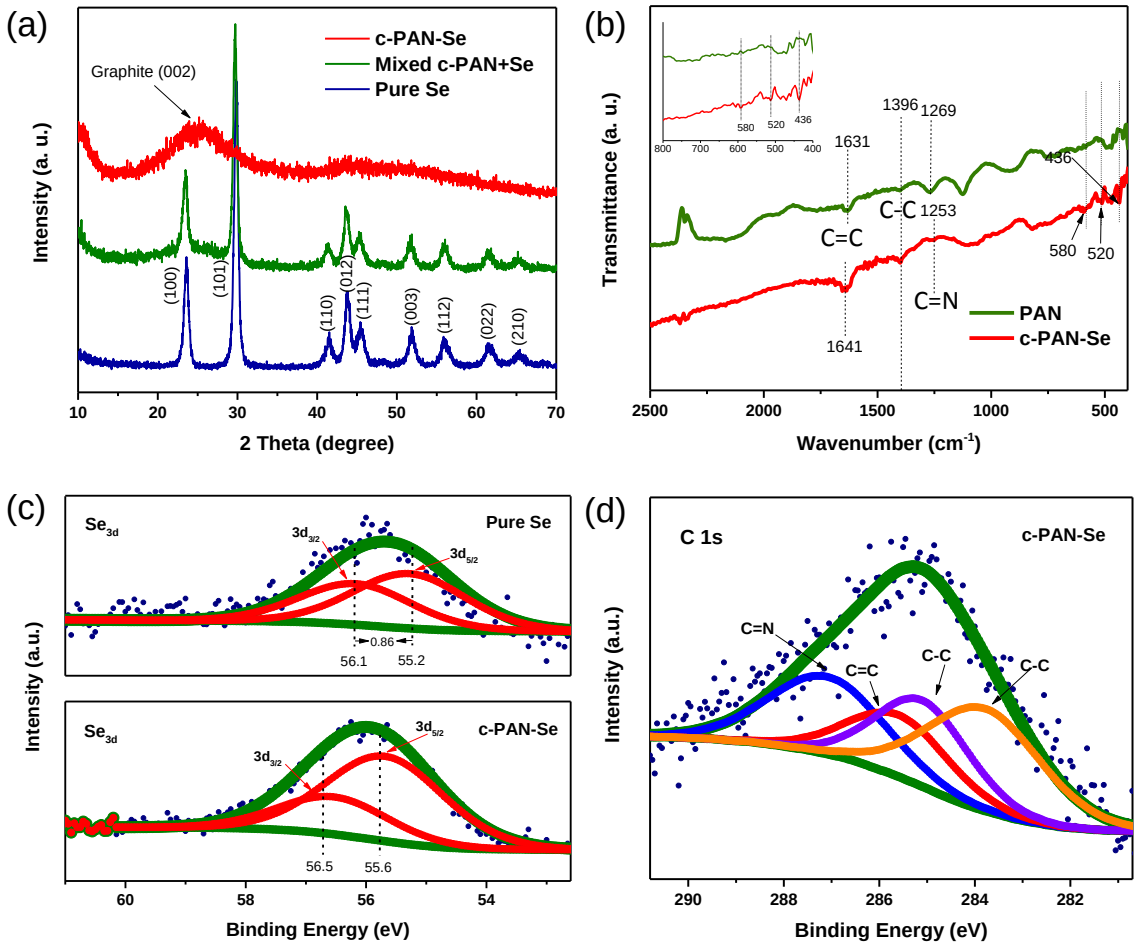

Figure 2. (a) XRD patterns of c-PAN-Se, mixed c-PAN+Se, and pure Se; (b) FT-IR spectra of carbonized-PAN and c-PAN-Se, with the inset showing an enlargement of the low wavenumber range; (c) XPS spectra of Se 3d for pure Se and c-PAN-Se; (d) XPS spectrum of C 1s for c-PAN-Se.

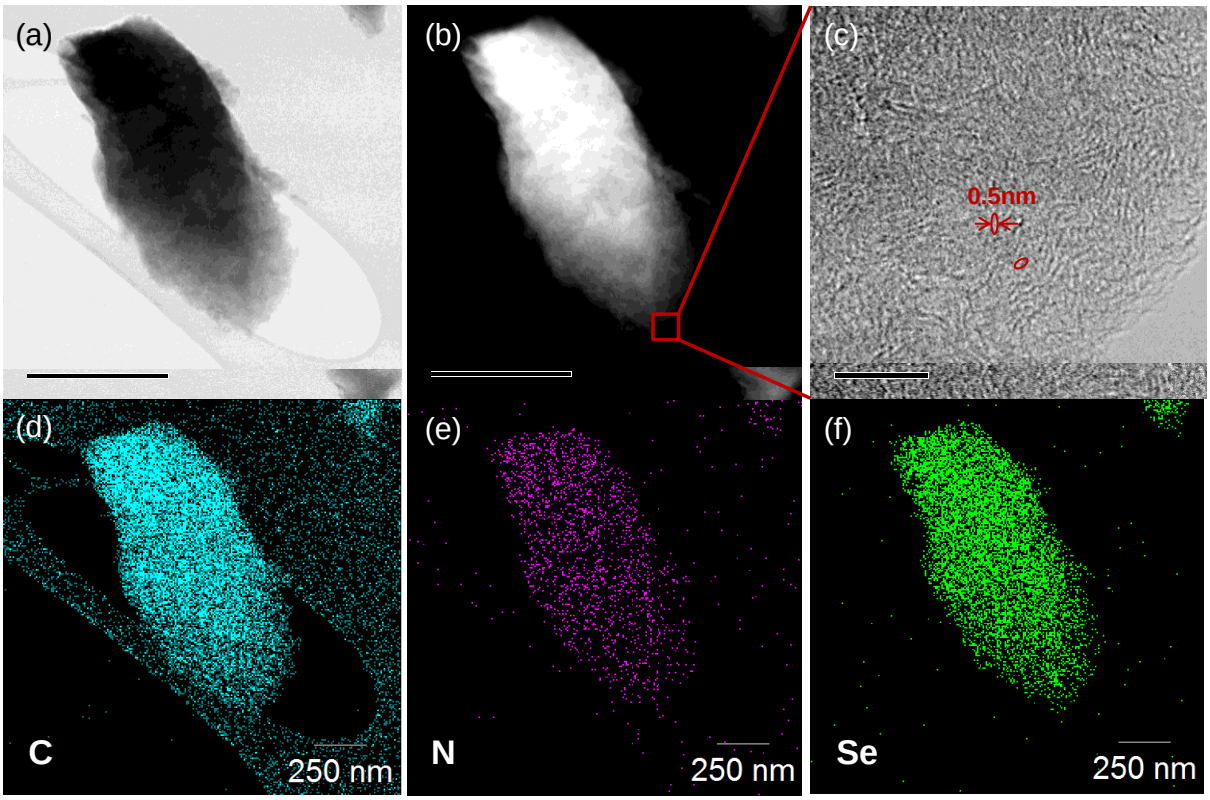

Figure 3. (a, b) TEM images of synthesized selenium/carbonized-PAN composite (c-PAN-Se); (c) high-resolution TEM image of the indicated region of c-PAN-Se in (b); (d-f) scanning TEM (STEM) images with EDX elemental mapping of carbon, nitrogen, and selenium.

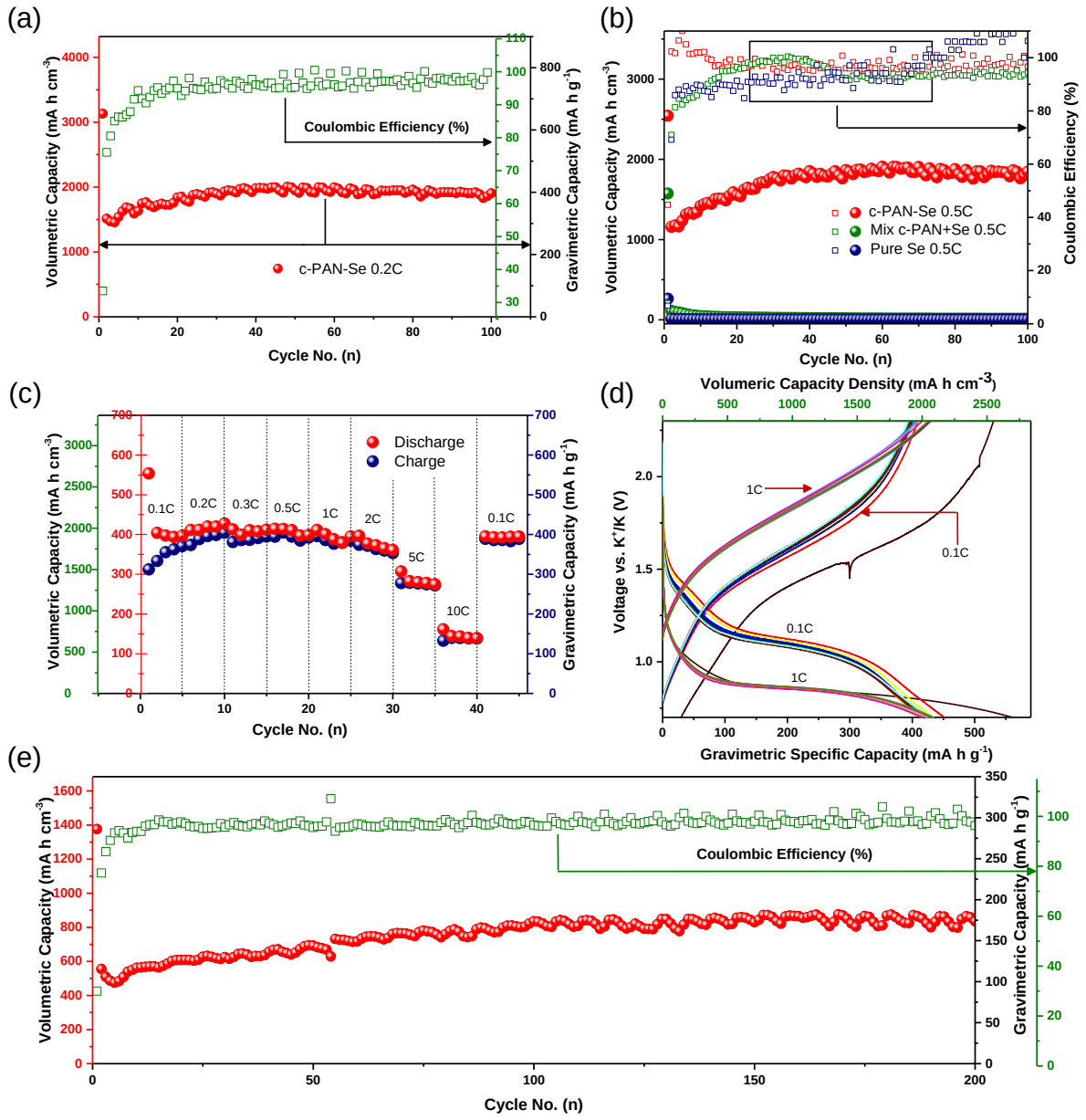

Figure 4. Electrochemical performance of the c-PAN-Se composite cathode in the voltage range of 2.3-0.7 V (vs. K^+/K): (a) cycling performance and coulombic efficiency of c-PAN-Se composite at 0.2 C; (b) Comparison of the cycling performance and coulombic efficiency among c-PAN-Se, physically mixed c-PAN+Se, and pure Se; (c) rate capabilities of c-PAN-Se from 0.1 C to 10 C; (d) Discharge/charge profiles at 0.1 C and 1 C; (e) Prolonged cycling performance of c-PAN-Se at the rate of 5 C.

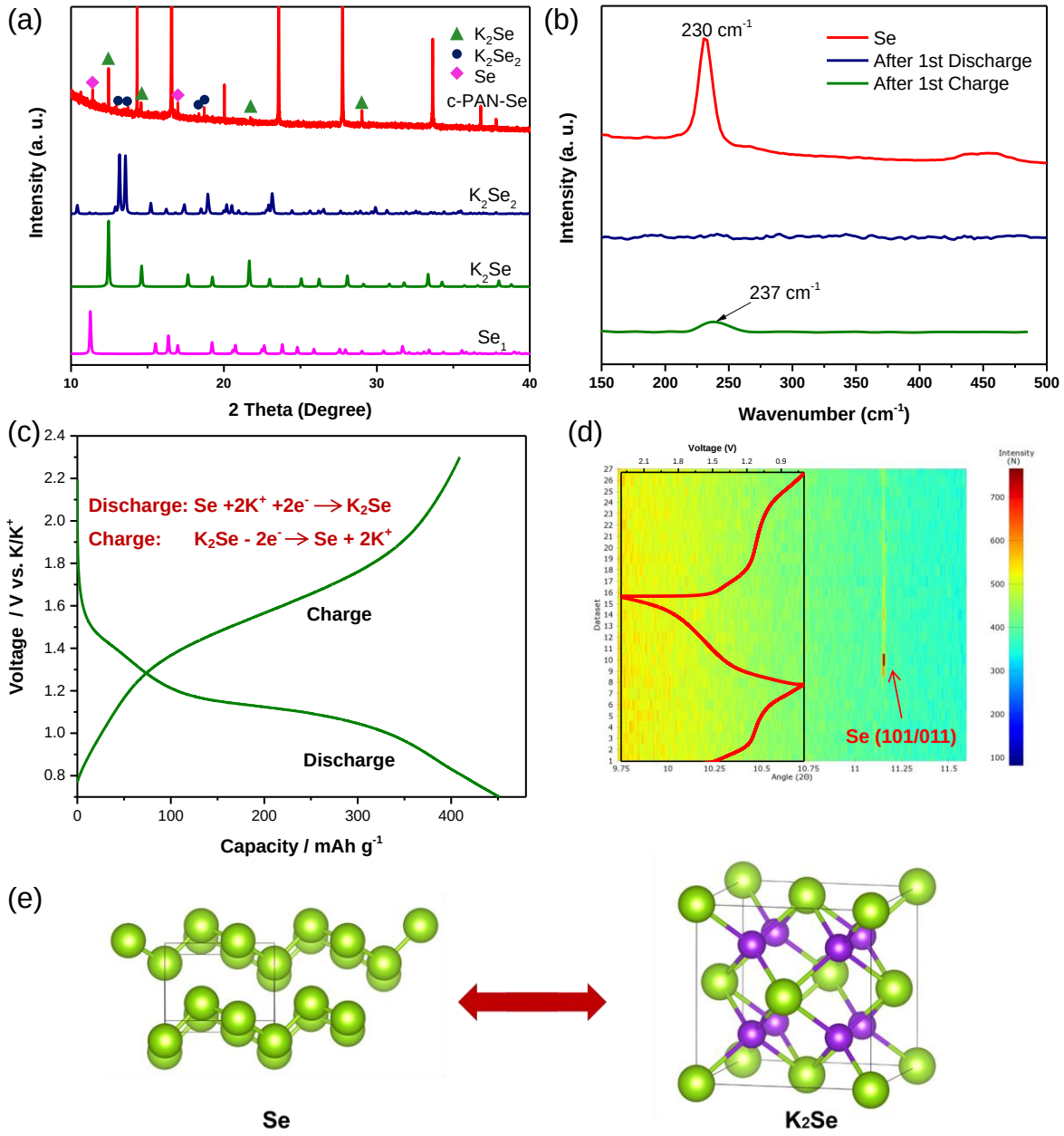

Figure 5. (a) High energy XRD (HEXRD) pattern of c-PAN-Se after the third full discharge, along with the standard patterns of Se, K_2Se, and K_2Se_2, collected with the same wavelength of 0.5899 Å as the c-PAN-Se electrode; (b) Ex-situ Raman characterization of c-PAN-Se; (c) Charge/Discharge profiles of c-PAN-Se; (d) In-situ synchrotron XRD spectra and the corresponding voltage profile; (e) Structural representations of the Se and K_2Se phases.